

# Suppressing Interfacial Recombination with a Strong-Interaction Surface Modulator for Efficient Inverted Perovskite Solar Cells

Bowei Li, Jun Deng, Joel A. Smith, Pietro Caprioglio, Kangyu Ji, Deying Luo, James D. McGettrick, K. D. G. Imalka Jayawardena, Rachel C. Kilbride, Aobo Ren, Steven Hinder, Jinxin Bi, Thomas Webb, Igor Marko, Xueping Liu, Yuren Xiang, Josh Reding, Hui Li, Shixuan Du, David G. Lidzey, Samuel D. Stranks, Trystan Watson, Stephen Sweeney, Henry J. Snaith, S. Ravi P. Silva,\* and Wei Zhang\*


Successful manipulation of halide perovskite surfaces is typically achieved via the interactions between modulators and perovskites. Herein, it is demonstrated that a strong-interaction surface modulator is beneficial to reduce interfacial recombination losses in inverted (p-i-n) perovskite solar cells (IPSCs). Two organic ammonium salts are investigated, consisting of 4-hydroxyphenethylammonium iodide and 2-thiopheneethylammonium iodide (2-TEAI). Without thermal annealing, these two modulators can recover the photoluminescence quantum yield of the neat perovskite film in contact with fullerene electron transport layer (ETL). Compared to the hydroxyl-functionalized phenethylammonium moiety, the thienylammonium facilitates the formation of a quasi-2D structure onto the perovskite. Density functional theory and quasi-Fermi level splitting calculations reveal that the 2-TEAI has a stronger interaction with the perovskite surface, contributing to more suppressed non-radiative recombination at the perovskite/ETL interface and improved open-circuit voltage ( $V_{OC}$ ) of the fabricated IPSCs. As a result, the  $V_{OC}$  increases from 1.11 to 1.20 V (based on a perovskite bandgap of 1.63 eV), yielding a power conversion efficiency (PCE) from  $\approx 20\%$  to 21.9% (stabilized PCE of 21.3%, the highest reported PCEs for IPSCs employing poly[N,N''-bis(4-butylphenyl)-N,N''-bis(phenyl)benzidine] as the hole transport layer, alongside the enhanced operational and shelf-life stability for unencapsulated devices.

## 1. Introduction

Inverted (p-i-n) perovskite solar cells (IPSCs) have a promising future among the emerging thin-film photovoltaics thanks to their plethora of applications, such as indoor,<sup>[1]</sup> wearable,<sup>[2]</sup> and tandem electronics.<sup>[3]</sup> For single-junction cells, the power conversion efficiencies (PCEs) have shown a significant increase from 3.9% in 2013<sup>[4]</sup> to a certified 24.3%<sup>[5]</sup> and the highest value of 25.37% most recently.<sup>[6]</sup> Despite remarkable progress, IPSCs have not yet achieved their full potential due to the notorious non-radiative recombination losses at the perovskite/fullerene interface,<sup>[7–9]</sup> thereby impairing the quasi-Fermi level splitting (QFLS) and device open-circuit voltage ( $V_{OC}$ ). Thus, introducing a modulator on the perovskite surface to control the semiconductor bulk termination is regarded as an efficient strategy to reduce recombination.<sup>[5,10–15]</sup>

In the past few years, surface defects have attracted much attention, which can

B. Li, K. D. G. I. Jayawardena, A. Ren, J. Bi, T. Webb, X. Liu, Y. Xiang, J. Reding, H. Li, S. R. P. Silva, W. Zhang  
Advanced Technology Institute  
Department of Electrical and Electronic Engineering  
University of Surrey  
Guildford GU2 7XH, UK  
E-mail: s.silva@surrey.ac.uk; wz0003@surrey.ac.uk

 The ORCID identification number(s) for the author(s) of this article can be found under <https://doi.org/10.1002/aenm.202202868>.

© 2022 The Authors. Advanced Energy Materials published by Wiley-VCH GmbH. This is an open access article under the terms of the Creative Commons Attribution License, which permits use, distribution and reproduction in any medium, provided the original work is properly cited.

DOI: 10.1002/aenm.202202868

J. Deng, H. Li, S. Du  
Beijing National Laboratory for Condensed Matter Physics  
Institute of Physics  
Chinese Academy of Sciences  
Beijing 100190, China

J. A. Smith, P. Caprioglio, H. J. Snaith  
Clarendon Laboratory  
Department of Physics  
University of Oxford  
Oxford OX1 3PU, UK

K. Ji, S. D. Stranks  
Cavendish Laboratory  
University of Cambridge  
Cambridge CB3 0HE, UK

D. Luo  
Department of Materials Science and Engineering  
University of Toronto  
Toronto M5G 3E4, Canada

induce deep-level traps and annihilate charge carriers within the perovskite bandgap.<sup>[16]</sup> To mitigate the detrimental surface defects, various so-called “passivators” or “passivating agents” have sprung up.<sup>[10,12,17]</sup> However, rationally tuning such passivation layers is challenging due to the complex chemical environment and electronic structure of the perovskite surface. Recent progress in IPSCs suggests the importance of energy level matching between perovskite and charge transport layer to ensure facilitated charge extraction in addition to the passivation effect.<sup>[8,15]</sup> For example, reducing the electron energetic barrier<sup>[13]</sup> or increasing the hole blocking<sup>[18]</sup> at the perovskite/electron transport layer (ETL) interface contributes to high-performance devices. Therefore, it is necessary to distinguish the effect of the surface modulators and their actual function site, such as on perovskite or at the interface, when associating with fullerene ETL.

Previous studies reported that molecules with certain functional groups, such as alkyl, phenyl, and charged ammonium salts, have shown excellent passivation on perovskite surfaces.<sup>[10,17]</sup> The electron-donating groups could further strengthen this effect.<sup>[17,19]</sup> Inspired by these and our findings,<sup>[20,21]</sup> we selected two organic halide salts, 4-hydroxyphenethylammonium iodide (HO-PEAI), and 2-thiopheneethylammonium iodide (2-TEAI), as the surface modulators in this study. Aside from the identical alkylammonium chain, HO-PEAI possesses a hydroxyl group as the para substituent while 2-TEAI has a thienyl instead of phenol moiety. These two surface modulators can regulate the perovskite film as evidenced by X-ray photoelectron spectroscopy (XPS), contact angle measurements, scanning electron microscopy (SEM), carrier lifetime mapping, and ultraviolet photoelectron spectroscopy (UPS). Moreover, 2-TEAI showed a stronger interaction than HO-PEAI, forming a quasi-2D structure on the perovskite surface without further annealing. This is corroborated by X-ray diffraction (XRD) and grazing-incidence wide-angle X-ray scattering (GIWAXS) measurements. The strong interaction between 2-TEAI and perovskite surface can be ascribed to the more negative adsorption energy as calculated by density functional theory (DFT). Further measurements of photoluminescence quantum yield (PLQY) and QFLS revealed that the 2-TEAI suppresses non-radiative recombination at the perovskite/ETL interface. This was supported by the

characterizations of light-dependent photo-responses, transient photovoltage (TPV), electrochemical impedance spectroscopy (EIS), and external quantum efficiency of electroluminescence (EQE<sub>EL</sub>). Based on the 2-TEAI treatment, high-performance IPSCs were obtained, yielding a  $V_{OC}$  of 1.20 V, a fill factor (FF) of 0.83, and a PCE of 21.9%, with the perovskite bandgap of 1.63 eV. In addition to photovoltaic parameters, the 2-TEAI also enhanced the stability of the unencapsulated devices, including stabilized operation (180 min, tracking at 1 Sun under ambient environmental conditions with 44–49% relative humidity, RH) and shelf-life stability (1500 h, stored at dark in an N<sub>2</sub>-filled glove box).

## 2. Results and Discussion

### 2.1. Characterization of Perovskite Thin Films

HO-PEAI and 2-TEAI (Figure S1, Supporting Information) were chosen as the candidates for the surface modulators. Both have a high dipole moment (15.13 and 13.11 D, see in Table S1, Supporting Information), indicative of a dense van der Waals interaction amongst them. Further calculation shows a more uniform distribution of electrostatic potential (ESP) in 2-TEAI (Figure S2, Supporting Information). We then characterized such materials by dynamically spin-coating (without additional annealing) onto the surface of a triple-cation lead binary-halide perovskite films (Cs<sub>0.05</sub>FA<sub>0.79</sub>MA<sub>0.16</sub>PbBr<sub>0.6</sub>I<sub>2.4</sub>, where Cs, FA, and MA are cesium, formamidinium, and methylammonium cations, respectively). This is shown schematically in **Figure 1a**, with **Figure 1b,c** being the chemical structures of HO-PEAI and 2-TEAI. Here, the optimized concentrations of these two modulators were determined as shown in **Figures S3 and S4**, Supporting Information. These modulators can affect the surface energy of the perovskite films. As seen in **Figure 1d–f**, the contact angle of water on the pristine perovskite film is 51.8°, dramatically increasing to 77.2° and 74.4° for the HO-PEAI and 2-TEAI, respectively. The increased contact angle could be caused by the hydrophobic organic moieties in these two modulators,<sup>[18]</sup> suggesting improved water and humidity resilience of the treated perovskite films. The modification of the perovskite films with HO-PEAI and 2-TEAI was also confirmed by SEM

J. D. McGettrick, T. Watson  
SPECIFIC

College of Engineering  
Swansea University  
Swansea SA1 8EN, UK

R. C. Kilbride  
Department of Chemistry  
University of Sheffield  
Sheffield S3 7HF, UK

A. Ren  
Institute of Fundamental and Frontier Sciences  
University of Electronic Science and Technology of China  
Chengdu 610054, China

S. Hinder  
The Surface Analysis Laboratory  
Department of Mechanical Engineering Sciences  
University of Surrey  
Guildford GU2 7XH, UK

I. Marko, S. Sweeney  
Advanced Technology Institute  
Department of Physics  
University of Surrey  
Guildford GU2 7XH, UK

D. G. Lidzey  
Department of Physics and Astronomy  
University of Sheffield  
Sheffield S3 7RH, UK

S. D. Stranks  
Department of Chemical Engineering and Biotechnology  
University of Cambridge  
Cambridge CB3 0AS, UK

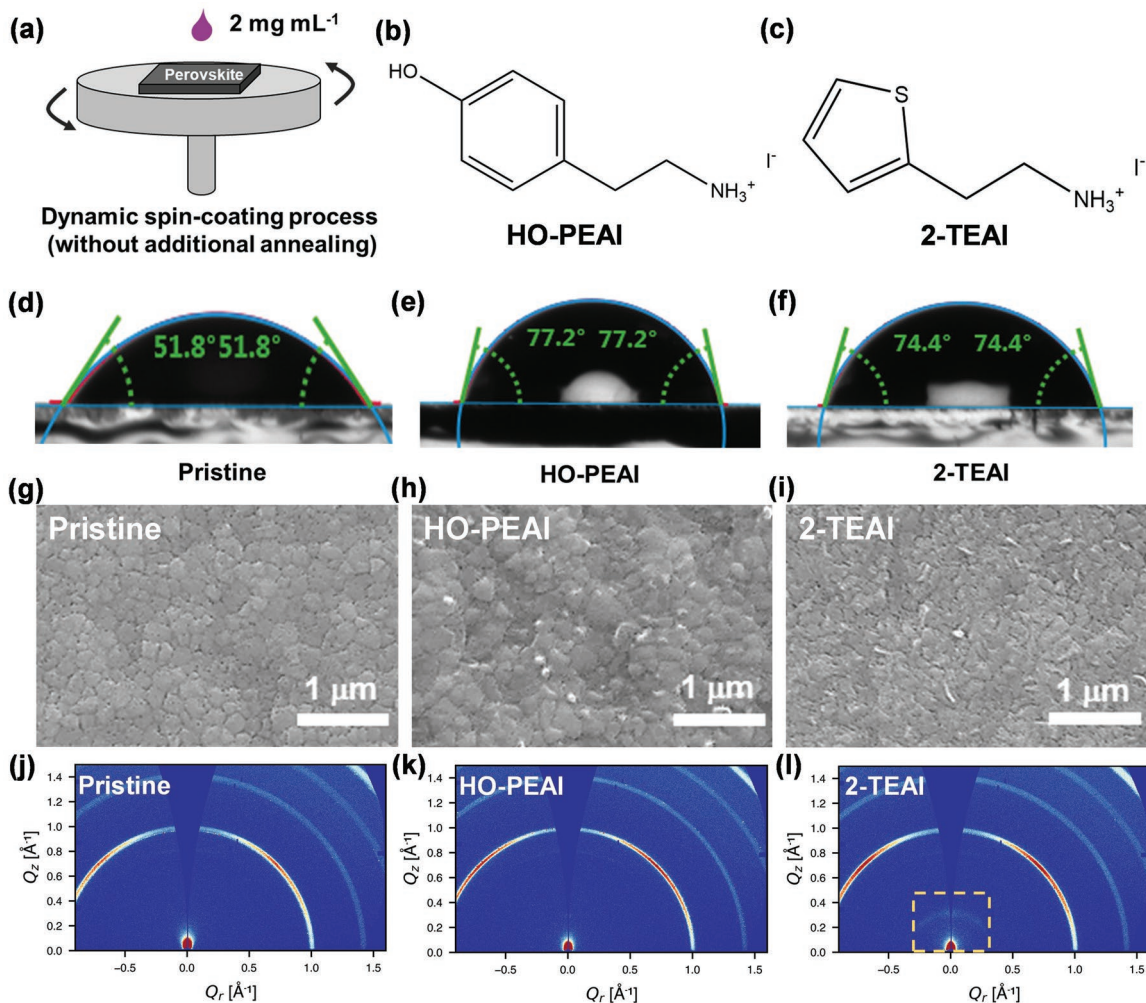


**Figure 1.** Properties of perovskite films without and with surface modulators. a) Preparation process. b,c) Chemical structure of HO-PEAI and 2-TEAI. d–f) Contact angles. The figures were captured at 5 s after dropping water on the perovskite surface. g–i) Top-view SEM images. j–l) 2D GIWAXS patterns collected with an incidence angle of 0.3° (penetration depth of ≈50 nm, details in Supporting Information). Note that the yellow square highlights the weak scattering ring caused by the quasi-2D structure.

imaging, where different surface morphologies can be observed in Figure 1g–i.

To characterize both bulk and surface film quality, XRD and GIWAXS measurements were conducted. All perovskite films have similar diffraction patterns, suggesting a well-crystallized photoactive 3D phase (Figure S5, Supporting Information). Here, the dominant peaks are assigned to the cubic (100), (110), (111), (200), (210), (211) crystal planes, respectively.<sup>[18]</sup> As all films were deposited on ITO glass, the (211) plane of the perovskite film is close to the (400) reflection from ITO at ≈35.2° (Figure S6a, Supporting Information).<sup>[22]</sup> Interestingly, a peak was detected at an angle of ≈4.1° for the 2-TEAI-treated perovskite film. This peak position is neither consistent with the pattern of pure 2-TEAI (Figure S6b, Supporting Information) nor 2D (2-TEAI)<sub>2</sub>PbI<sub>4</sub> (Figure S6c, Supporting Information), but instead is close to the characteristic “*n* = 2” quasi-2D structure (nominally having the composition of (2-TEAI)<sub>2</sub>FAPb<sub>2</sub>I<sub>7</sub>).<sup>[23]</sup> This finding is further verified by surface-sensitive GIWAXS data (Figure 1j–l), in which a weak scattering ring (highlighted

yellow box) appears a tiny peak in the 1D integrated data (Figure S7, Supporting Information). In contrast, this was not observed in the HO-PEAI-treated sample, suggesting 2-TEAI has a stronger interaction with the perovskite surface.

To investigate the possible interaction between the surface modulators and perovskite films, we performed DFT calculations. Here, for simplifying the calculations, a cubic formamidinium lead halide (FAPbI<sub>3</sub>) model was used as a representative surface to describe triple-cation perovskite. As the organic cations in perovskite composition can be volatilized via thermal annealing, we investigated a PbI<sub>2</sub>-terminated surface that provides a dominant reservoir for trap states.<sup>[10,24]</sup> To eliminate these electronic traps, the introduced modulator species is assumed to interact with the perovskite surface through different types of bonds (e.g., coordinate, ionic, hydrogen, and halogen).<sup>[16,25]</sup> Hence, two possible interactions were studied separately based on the chemical structure of each modulator. The iodide ions in the modulators are expected to compensate for iodide vacancies and stabilize the PbI<sub>6</sub> octahedra in perovskite whilst the oxygen

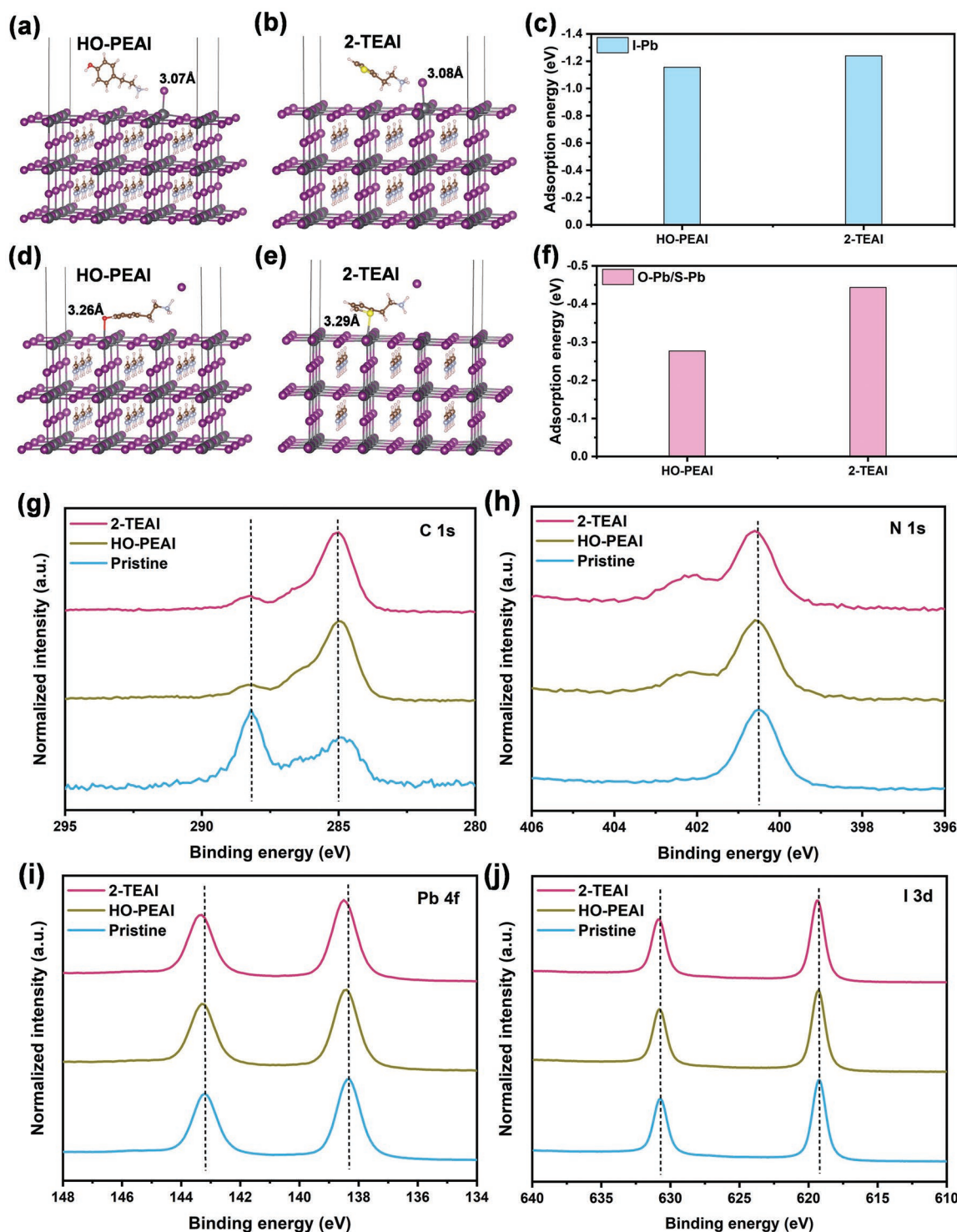


**Figure 2.** Interactions between surface modulators and perovskite films. Theoretical models of HO-PEAI and 2-TEAI on the PbI<sub>2</sub>-terminated surface of FAPbI<sub>3</sub>, consisting of optimized geometrical structures through a,b) I–Pb bond and d,e) O–Pb/S–Pb bond; c,f) Corresponding adsorption energies (see more details in Supporting Information). g–j) High-resolution XPS core-level spectra of perovskite films without and with surface modulators, consisting of C 1s, N 1s, Pb 4f, and I 3d. Note that all these perovskite films were deposited on ITO glass/poly-TPD.

(O) or sulfur (S) atoms are expected to interact with the Pb<sup>2+</sup> ions (Figures S8 and S9, Supporting Information). Figure 2a,b shows the I–Pb interaction between modulator and perovskite, with

a calculated bond length of 3.07 Å for HO-PEAI and 3.08 Å for 2-TEAI. The corresponding adsorption energy ( $\Delta E_{\text{ads}}$ ) is shown in Figure 2c. As a result of lower  $\Delta E_{\text{ads}}$  (–1.24 vs –1.16 eV, see

details in Table S2, Supporting Information), the 2-TEAI is expected to be more readily adsorbed on the perovskite surface. Furthermore, the lone pair of electrons in O and S is expected to coordinate with the perovskite as shown in Figure 2d,e. The calculated  $\Delta E_{\text{ads}}$  ( $-0.28$  vs  $-0.44$  eV, see details in Table S3, Supporting Information) also indicates the preferential adsorption of 2-TEAI (Figure 2f). Further calculated charge density difference (CDD) and electron localization function (ELF) values confirm that both interactions are prone to occur (Figure S10, Supporting Information). In comparison with HO-PEAI, the DFT results demonstrate that the 2-TEAI undergoes a stronger interaction with the perovskite surface. This interaction was also studied by conducting XPS (Figure S11, Supporting Information). As shown in Figure 2g–j, high-resolution C 1s, N 1s, and S 2p (Figure S12, Supporting Information) spectra confirmed the surface modification by these modulators. After treatment, the C=O peak (288.2 eV) shows a suppressed intensity, suggesting the improved moisture resistance.<sup>[26]</sup> This is consistent with the increased contact angles as discussed above. A new peak is seen at 402.2 eV,<sup>[27]</sup> indicative of the quaternary amine in the spin-coated HO-PEAI

and 2-TEAI layers. The larger shift of binding energies (N 1s, Pb 4f, and I 3d core levels) indicated the enhanced interaction between 2-TEAI and the perovskite surface. Due to such a strong interaction, 2-TEAI is likely to attach at the A sites in an  $\text{ABX}_3$  perovskite, leading to the formation of the quasi-2D structure as confirmed by the above XRD and GIWAX results.

To further confirm the function of modulators, we performed a series of optical measurements. We find that these two surface modulators do not alter the absorption spectra of perovskite films as is evidenced from the corresponding  $T_{\text{auc}}$  plot with an optical bandgap of 1.63 eV in both cases (Figure S13, Supporting Information). Carrier lifetime maps determined using confocal fluorescence microscopy indicate an improved lifetime after surface treatments (Figure S14, Supporting Information). To accurately distinguish the effect of the modulators on the perovskite or at the perovskite/ETL interface, we measured the PLQY of perovskite films without and with contacting to [6,6]-phenyl-C<sub>61</sub>-butyric acid methyl ester (PC<sub>61</sub>BM, abbreviated as PCBM in the figure and following sections). In Figure 3a, the PLQY results show that the surface modulators do not strongly

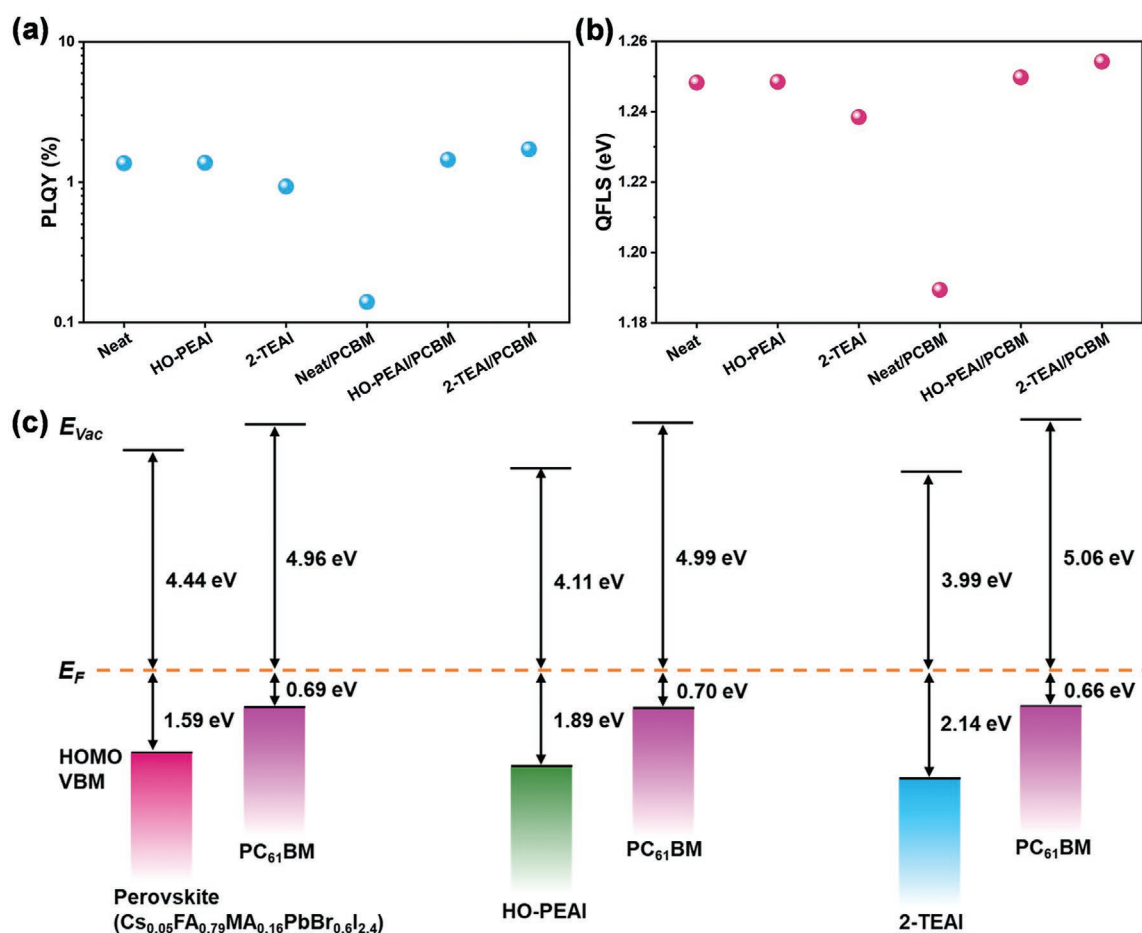


**Figure 3.** Optical and electronic properties of perovskite films without and with surface treatment (2 mg mL<sup>-1</sup> HO-PEAI or 2-TEAI). a) PLQY and b) QFLS of different types of films deposited on the bare glass. “Neat” denotes the structure of glass/perovskite, with “HO-PEAI” and “2-TEAI” referring to the structure of glass/perovskite/modulator. “Neat/PCBM” indicates the half stack structure of glass/perovskite/PCBM, with “HO-PEAI/PCBM” and “2-TEAI/PCBM” denoting glass/perovskite/modulator/PCBM samples. c) Energy levels of the perovskites/PCBM interface.  $E_{\text{vac}}$  is vacuum level,  $E_{\text{F}}$  is Fermi level. HOMO is the highest occupied molecular orbital and VBM is the valence band maximum. Note that the data were obtained from the UPS measurements based on four to five different areas for each sample and the sample details were shown in Table S4, Supporting Information.

affect the luminescence of the neat perovskite (which is found to be in the 1% regime), indicating an absence of direct passivation on the perovskite surface. However, as expected from previous reports,<sup>[8,28]</sup> a strong reduction of the PLQY is observed when the perovskite is coated with the PCBM, indicating the generation of non-radiative recombination at this interface. Importantly, when the perovskite surface is first treated with surface modulators, the PLQY of perovskite/PCBM stacks is completely recovered, approaching that of the pure perovskite ( $\approx 1\%$ ). Using the measured PLQY values, we can calculate the QFLS as described in Figure S15, Supporting Information. In Figure 3b, the neat perovskite exhibits a QFLS of  $\approx 1.25$  eV, which is then reduced to 1.19 eV on contact with the PCBM. The surface modulators return the QFLS to 1.25 eV for the half-stack case (perovskite/PCBM). We thus conclude that the interfacial recombination is dramatically suppressed by HO-PEAI and 2-TEAI. In particular, the higher QFLS than neat and HO-PEAI suggests that 2-TEAI is a superior modulator, and its major role is in suppressing non-radiative recombination, specifically at the perovskite/PCBM interface. The electronic structure between perovskite and PCBM was investigated by UPS (see details in Table S4, Supporting Information). As illustrated

in Figure 3c, the 2-TEAI induces a deeper valence band edge, which is expected to provide a stronger hole-blocking effect at the perovskite/PCBM interface and thus is more beneficial for reducing the interfacial recombination. Based on these results, we believe the 2-TEAI would enhance the  $V_{OC}$  of manufactured PSCs.

## 2.2. Photovoltaic Performance of 2-TEAI-Treated Devices

To test our hypothesis, we fabricated p-i-n planar devices based on the hole transport layer (HTL) of poly [*N,N'*-bis(4-butylphenyl)-*N,N'*-bis(phenyl)benzidine] (poly-TPD). In the fabrication process (Figure 4a), [2-(9H-carbazol-9-yl)ethyl] phosphonic acid (2PACz)<sup>[29]</sup> was spin-coated on the poly-TPD to enable full coverage of the perovskite films (see details in Figures S16 and S17, Supporting Information). The UPS performed at each stage suggests that the 2PACz can decrease the energy barrier between poly-TPD and perovskite (see Figure 4b). Following this, a 2 mg mL<sup>-1</sup> 2-TEAI solution was spin-coated on the perovskite surface, which can block hole transport between perovskite and PCBM. As shown in

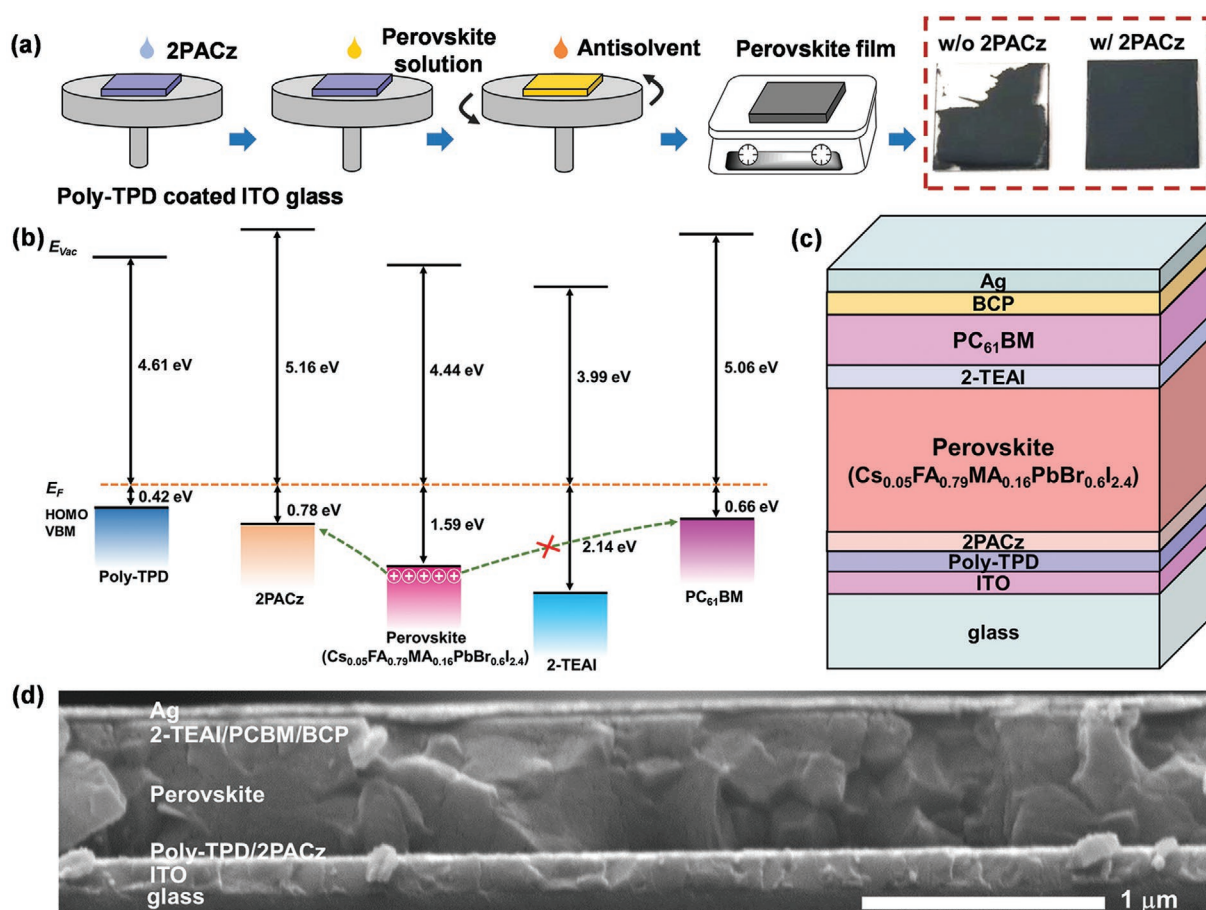


**Figure 4.** Inverted perovskite solar cells based on the 2-TEAI treatment. a) Preparation of perovskite films on poly-TPD coated ITO glass. The 2PACz layer is introduced to overcome the de-wetting issue of the hydrophobic poly-TPD. b) Band edge positions of functional layers extracted from UPS measurements. “Poly-TPD” is glass/ITO/poly-TPD. “2PACz” is glass/ITO/poly-TPD/2PACz. “Perovskite” is glass/ITO/poly-TPD/2PACz/perovskite. “2-TEAI” is glass/ITO/poly-TPD/2PACz/perovskite/2-TEAI. “PCBM” is glass/ITO/poly-TPD/2PACz/perovskite/2-TEAI/PCBM. c) Schematic configuration of the device architecture. d) Cross-sectional SEM image of a completed device.

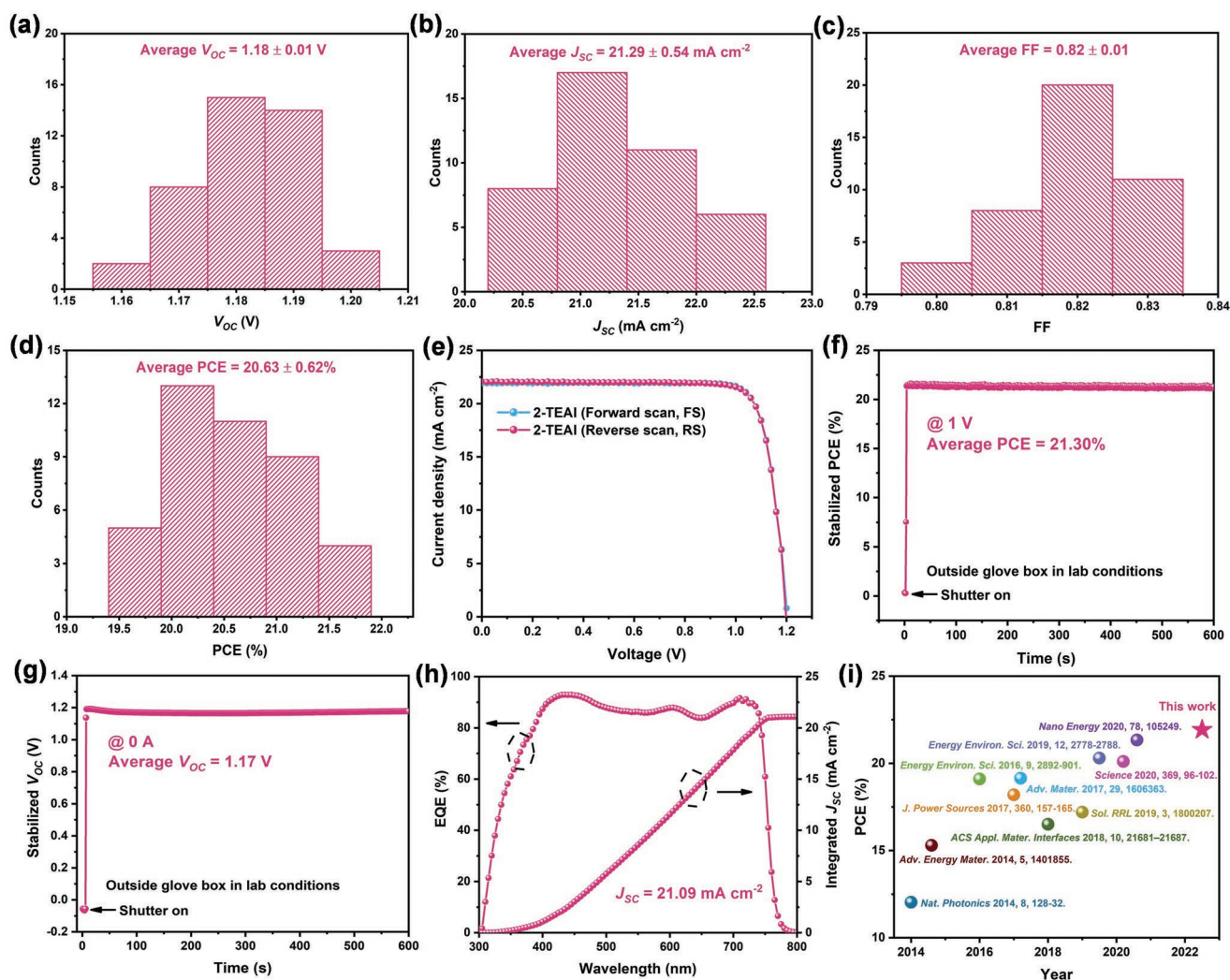


**Figure 5.** Performance of 2-TEAI devices. a–d) Statistical photovoltaic parameters of devices, including histogram of the  $V_{OC}$ ,  $J_{SC}$ , FF, and PCE. Note that the data were collected from 42 devices. The devices were measured outside the glove box under simulated AM 1.5G solar irradiation at  $100 \text{ mW cm}^{-2}$  with an aperture area of  $0.09 \text{ cm}^2$ . For each device, the data shown here are the average values of the forward and reverse scans. e)  $J$ – $V$  curves of the champion device, consisting of the forward scan (FS,  $-0.2$  to  $1.2 \text{ V}$ ) and reverse scan (RS,  $1.2$  to  $-0.2 \text{ V}$ ). f) The stabilized PCE as a function of illumination time, measured by holding at the  $V_{MPP}$  of  $1 \text{ V}$ . g) The stabilized  $V_{OC}$  as a function of illumination time, measured by holding the current at  $0 \text{ A}$ . Note that all these stabilized data were recorded every  $1 \text{ s}$ . h) Corresponding EQE spectrum for the champion cell. i) Summarized PCEs for inverted PSCs based on poly-TPD in the literature, with all data summarized in Table S6, Supporting Information.

Figure 4c,d, the devices fabricated have a structure of glass/ITO/poly-TPD/2PACz/perovskite/2-TEAI/PCBM/bathocuproine (BCP)/Ag.

To accurately quantify the photovoltaic performance of this architecture, 42 devices were fabricated in separate batches and then characterized, with current–voltage sweep characteristics listed in Table S5, Supporting Information. We find little difference between the forward- and reverse-scan data, indicating very little hysteresis in the 2-TEAI devices. Figure 5a–d shows histograms of key device parameters, in which the  $V_{OC}$  ranges from  $1.16$  to  $1.20$  with an average of  $1.18 \pm 0.01 \text{ V}$  (arithmetic mean  $\pm$  standard deviation) and the FFs are distributed between  $0.80$  to  $0.84$  with an average of  $0.82 \pm 0.01$ . This leads to an average PCE of  $20.63 \pm 0.62\%$ . It is noteworthy that the champion device achieved a  $V_{OC}$  of  $1.20 \text{ V}$  with a PCE of

$21.92\%$  (reverse) and  $21.85\%$  (forward), respectively (Figure 5e and Figure S18, Supporting Information). As listed in Table 1, the PCE enhancement found for the 2-TEAI devices is mainly attributed to the dramatically improved  $V_{OC}$ , in agreement with the expected reduction of interfacial losses as determined from our spectroscopic studies.

The efficiency obtained from  $J$ – $V$  curves is a non-steady-state value as it is readily affected by transient processes within a device.<sup>[30]</sup> To verify the champion values of PCEs determined, we measured the stabilized power output at the voltage of maximum power point ( $V_{MPP}$ ). As shown in Figure 5f, the stabilized PCE attained an average value of  $21.30\%$  over  $600 \text{ s}$  of continuous illumination. The difference between the stabilized PCE and the  $J$ – $V$  scanned PCE can be quantified by the “fidelity” of the  $J$ – $V$  scan, defined as the steady-state PCE divided by the

**Table 1.** The photovoltaic parameters of champion devices measured outside the glove box under simulated AM 1.5G solar irradiation at 100 mW cm<sup>-2</sup>. For each device, the *J*-*V* curves were only scanned once, consisting of the forward scan (FS, -0.2 to 1.2 V) and reverse scan (RS, 1.2 to -0.2 V). Note that the control device has a structure of glass/ITO/poly-TPD/2PACz/perovskite/PCBM/BCP/Ag and the 2-TEAI device has a structure of glass/ITO/poly-TPD/2PACz/perovskite/2-TEAI/PCBM/BCP/Ag. The integrated *J*<sub>SC</sub> is obtained from the EQE spectrum (see details in Figure S19, Supporting Information).

Sample	<i>V</i> <sub>OC</sub> [V]	<i>J</i> <sub>SC</sub> [mA cm <sup>-2</sup> ]	Integrated <i>J</i> <sub>SC</sub> [mA cm <sup>-2</sup> ]	FF	PCE [%]
Control (FS)	1.11	22.16	21.13	0.81	19.95
Control (RS)	1.12	22.19	–	0.81	19.97
2-TEAI (FS)	1.20	21.93	21.09	0.83	21.85
2-TEAI (RS)	1.20	22.09	–	0.83	21.92

scan-determined PCE.<sup>[30]</sup> Here, we calculate a fidelity of 0.97 for the 2-TEAI device. We have also determined stabilized device *V*<sub>OC</sub> over 600 s (see Figure 5g). The device is found to have an average stabilized *V*<sub>OC</sub> of 1.17 V, consistent with the statistical data shown in Figure 5a. Furthermore, we have verified the measured *J*<sub>SC</sub> value by determining EQE spectra (Figure 5h and Figure S19, Supporting Information). The integrated *J*<sub>SC</sub> was calculated to be 21.09 mA cm<sup>-2</sup>; a value that approaches the *J*<sub>SC</sub> obtained from *J*-*V* curves within 5% difference. We believe that the photovoltaic parameters determined for 2-TEAI devices are the best yet reported for IPSCs employing a poly-TPD transporting layer (Figure 5i and Table S6, Supporting Information).

We note that previous research has determined that alkylammonium salts can be used at the HTL/perovskite interface in p-i-n devices to improve efficiency.<sup>[31,32]</sup> We thus spin-coated 2-TEAI on top of the poly-TPD/2PACz. However, the resultant devices did not show improved performance even in a wide range of concentrations (Figure S20, Supporting Information). The reason could be attributed to the low non-radiative losses at the poly-TPD/perovskite interface as indicated by the PLQY and QFLS results (Figure S21, Supporting Information). Furthermore, unlike previous reports,<sup>[23,33]</sup> we did not use thermal annealing in the following deposition of 2-TEAI since it can impair the device *V*<sub>OC</sub> (Figure S22, Supporting Information). The advantage of this annealing-free process indicates that 2-TEAI surface treatment in our study is a facile and straightforward method.

We now discuss stability, which is another important factor in the solar-cell “golden triangle.”<sup>[34]</sup> To evaluate device stability, we measured long-term stabilized power output under lab conditions (44–49% RH), considering the combined effects of electrical bias, moisture, and illumination stresses.<sup>[30,35]</sup> Here, unencapsulated devices were continuously measured under AM 1.5G illumination using an AAA xenon arc lamp without a UV filter (equivalent to ISOS-L-1 protocol<sup>[35]</sup>). Temperature and humidity were continuously monitored (see Figure S23, Supporting Information). The stabilized PCE of 2-TEAI device is found to exhibit a much slower decay compared to the control device, maintaining 91% of its initial PCE after around 180 min. In contrast, the control device decreased to 53% of its initial PCE. The improved stability of 2-TEAI devices was also confirmed by the results of 1500 h of shelf-life storage

(ISOS-D-11<sup>[35]</sup>), where *J*<sub>SC</sub> and PCE only dropped by less 1%; a value that compares favorably to that of the control devices in which *J*<sub>SC</sub> and PCE reduced by 5% (see Figure S24, Supporting Information).

### 2.3. Mechanism of Performance Enhancement

To understand the mechanisms underlying the observed performance improvements, a series of characterization measurements were performed based on devices either with or without the 2-TEAI treatment. Figure S25, Supporting Information, shows the light-soaking-free and fast response for these two types of devices, implying the high reliability of their *J*-*V* curves. Furthermore, the *J*-*V* curves were also measured continuously under light intensities from 0.1 to 1 Sun. As shown in Figure 6a,b, both devices are almost hysteresis-free at each irradiation intensity (see more details in Figure S26, Supporting Information). The 2-TEAI device was found to have a higher FF than the control device even at weak light intensities (Figure 6c). With increasing light intensity, the *J*<sub>SC</sub> and *V*<sub>OC</sub> both exhibit a monotonic increase (Figure 6d,e). There are two dominant traps in the perovskite bandgap:<sup>[10,16]</sup> a) the shallow-level traps (like halide or organic vacancies) could induce the ion migration that is responsible for some unusual phenomena, such as hysteresis (discrepancy between the forward and reverse scan in *J*-*V* curves)<sup>[36]</sup> and light soaking effect (photoinduced improvement of device performance);<sup>[37]</sup> b) the deep-level traps (like undercoordinated Pb<sup>2+</sup> ions) would act as the non-radiative centers and annihilate free charge carriers through the non-radiative recombination. Based on our results, the control devices also show fast response and negligible hysteresis, indicating the low density of shallow traps. Thus, the function of 2-TEAI treatment is mainly focusing on the deep-level traps. The DFT and XPS results have demonstrated the strong interaction between 2-TEAI and undercoordinated Pb<sup>2+</sup> ions, and the improved device *V*<sub>OC</sub> will suggest the suppressed non-radiative recombination. Non-radiative recombination can be characterized by fitting the light intensity-dependent *V*<sub>OC</sub>. From the slope of this dependence, it is possible to extrapolate an ideality factor, which can be used to describe the dominant recombination process.<sup>[38]</sup> The 2-TEAI device had a lower ideality factor than the control device (1.39 vs 1.54), indicating suppressed non-radiative recombination. This result is also confirmed by TPV and EIS measurements. The 2-TEAI device had a much longer decay time (Figure 6f) and higher resistance (Figure S27, Supporting Information) than the control. These results demonstrated the reduced non-radiative losses in full PSC devices.

Compared to the control devices, the 2-TEAI devices show a marked increase in *V*<sub>OC</sub> under different light intensities or scan rates (Figures S26 and S28, Supporting Information). To explore this *V*<sub>OC</sub> improvement, we quantify the energy losses (see details in Figure S29, Supporting Information), by calculating the Δ*V*<sub>OC, nrad</sub> (non-radiative *V*<sub>OC</sub> loss).<sup>[39]</sup> In the preceding discussion, the 2-TEAI surface treatment is beneficial in reducing non-radiative recombination. Since the perovskite bandgap is unchanged before and after 2-TEAI treatment (see



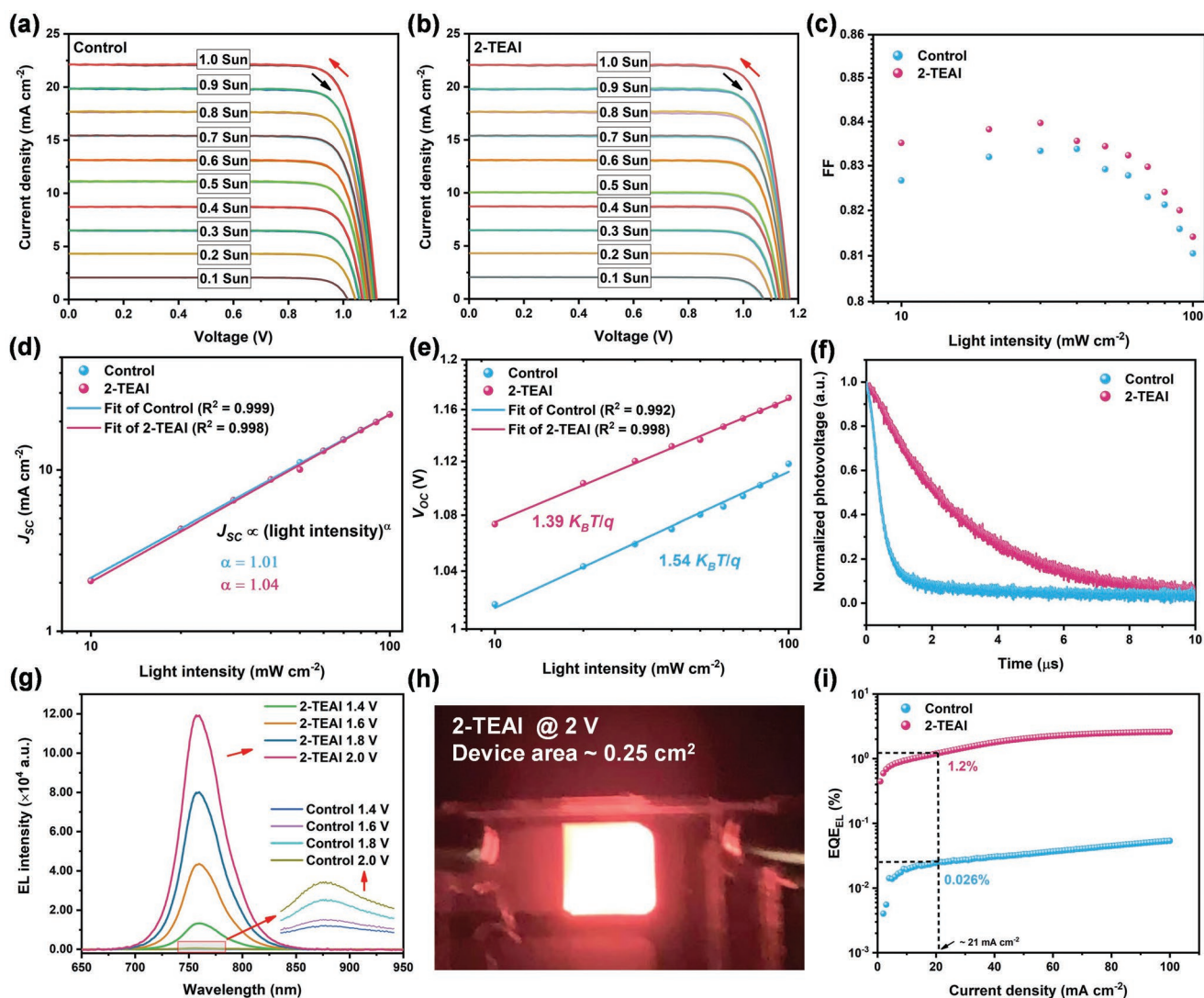


**Figure 6.** Characterization of devices without or with 2-TEAI treatment. a,b)  $J$ - $V$  curves measured under light intensities ranging from 0.1 to 1 Sun, consisting of reverse scan (RS, 1.2 to  $-0.2$  V) and forward scan (FS,  $-0.2$  to 1.2 V). For this measurement, the control used was the champion device (with a  $V_{OC}$  of 1.12 V,  $J_{SC}$  of 22.12  $\text{mA cm}^{-2}$ , FF of 0.81 and PCE of 20%, obtained from an average of the reverse and forward scan) while the 2-TEAI device was randomly selected (with a  $V_{OC}$  of 1.17 V,  $J_{SC}$  of 22.07  $\text{mA cm}^{-2}$ , FF of 0.82, and PCE of 21%, averaging parameters of both sweeps). Light intensity-dependent c) FF, d)  $J_{SC}$ , and e)  $V_{OC}$ . For each point, the data were the average values obtained from the forward and reverse scans. f) TPV decay curves. g) EL spectra of control and 2-TEAI devices under various bias voltages. h) Image of a 2-TEAI-treated device operating as an LED. i) EQE of EL spectra. Note that the devices are based on the structure of glass/ITO/poly-TPD/2PACz/perovskite/(with or without 2-TEAI)/PCBM/BCP/Ag. For TPV and EL measurements, the devices were randomly selected and their  $J$ - $V$  curves are shown in Supporting Information. All these measurements were conducted outside the glove box under ambient conditions.

details in Figure S30, Supporting Information), the enhanced  $V_{OC}$  will be mainly caused by a reduction in  $\Delta V_{OC, \text{nrad}}$ . To verify this, the EL spectra of these two devices operated as light-emitting diodes (LEDs) were compared. As shown in Figure 6g, we find that the 2-TEAI device emits EL emission with 200 times intensity than the control device at 2 V, with an image of the emission in Figure 6h. At one sun equivalent current injection ( $\approx 21 \text{ mA cm}^{-2}$ , obtained from  $J$ - $V$  curves in Figure S31, Supporting Information), the  $\text{EQE}_{EL}$  of the 2-TEAI device is 1.2% while the control device is only 0.026% (Figure 6i). Importantly, the peak emission wavelength position (759.5 nm) of

both devices does not shift as a function of applied voltages; a finding that confirms the material phase stability despite the 20% Br content (Br/I ratio) used in our perovskite composition. We calculated  $V_{OC}$  difference using  $\Delta V_{OC} = K_B T/q \ln(\text{EQE}_{EL, 2\text{-TEAI}}/\text{EQE}_{EL, \text{control}})$  and found  $\Delta V_{OC} = 0.099 \text{ V}$ ; a value in good agreement with the  $V_{OC}$  improvement determined from the  $J$ - $V$  curves (0.1 V, see Figure S31, Supporting Information). Using the equations, we find  $\Delta V_{OC, \text{nrad}}$  of the 2-TEAI device to be 0.11 V, which is lower than that of the control device (0.21 V). This reduction further confirms the suppressed non-radiative losses.

### 3. Conclusion

In summary, we introduced two organic halide salts, HO-PEAI and 2-TEAI, onto the surface of perovskite films through a facile spin-coating process without an additional annealing step. Briefly, the 2-TEAI is an efficient surface modulator that contributes to both efficiency and stability of the PSC devices. This is mainly due to a stronger interaction with the perovskite surface: forming a quasi-2D structure and reconfiguring the electronic energy level. These characteristics enable 2-TEAI to predominantly reduce the non-radiative recombination at the perovskite/PCBM interface. The findings suggest that the role of the modulator is more than surface passivation. Our study will provide insight into the selection and molecular design of post-treatment materials for highly efficient and stable perovskite solar cells.

### 4. Experimental Section

Experimental details are provided in the Supporting Information.

### Supporting Information

Supporting Information is available from the Wiley Online Library or from the author.

### Acknowledgements

W.Z. thanks the EPSRC standard research (EP/V027131/1) and the Newton Advanced Fellowship (192097) for financial support. B.L. thanks the China Scholarship Council (CSC, No. 201706020158) for financial support during his PhD career. K.D.G.I.J. and S.R.P.S. thank the European Commission H2020 CORNET program (Grant ID: 760949) and the Equal Opportunities Foundation Hong Kong for financial support. H.L. thanks the National Key Research and Development Program of China (2019YFB1503500), the State Key Laboratory of Metastable Materials Science and Technology (201901), and the Fujian Key Laboratory of Photoelectric Functional Materials (FJPFM-201902) for financial support. J.B. thanks the China Scholarship Council (CSC, No. 201808370197) for financial support. T.W. thanks the University of Surrey DCSA3 scholarship. J.D.M. and T.W. acknowledge funding from the EPSRC SPECIFIC IKC (EP/N020863/1). D.G.L. thanks the UK EPSRC for support via research grant EP/S009213/1 (The integration of photovoltaic devices with carbon-fiber composites). The authors thank the company Xenocs for their help and ongoing support with the X-ray scattering instrument based at The University of Sheffield and the EPSRC for funding the purchase of this instrument. K.J. and S.D.S. acknowledge funding from the Royal Society, the Engineering and Physical Sciences Research Council (EPSRC, EP/R023980/1 and EP/V027131/1) and the European Research Council (ERC) under the European Union's Horizon 2020 research and innovation program (HYPERION, Grant Agreement Number 756962). S.D.S. acknowledges funding from the Royal Society and Tata Group (UF150033).

### Conflict of Interest

D.G.L. is a co-director of the company Ossila that retails materials and equipment used in perovskite photovoltaic device research and development. H.J.S. is a cofounder, chief scientific officer, and a director of Oxford PV Ltd.

### Author Contributions

B.L. conceived the work, fabricated, and characterized solar cells; conducted SEM, UV-vis, and contact angle measurements. B.L. and K.D.G.I.J. conducted the EQE measurement. J.D. and S.D. conducted the DFT calculations. J.A.S. conducted the XRD measurement. P.C. conducted the PLQY and QFLS measurements. R.C.K. conducted the GIWAXS measurements and J.A.S. analyzed the data. K.J. conducted the carrier lifetime maps. S.H. conducted the XPS measurement. J.D.M. conducted the UPS measurements. K.D.G.I.J. and I.M. conducted the TPV measurements. T.W. conducted the EL measurements. A.R. conducted the EQE<sub>EL</sub> measurements. J.B. conducted the EIS measurements. B.L. wrote the draft of the paper and the other authors contributed to data interpretation or revision of the manuscript. W.Z. and S.R.P. directed and supervised the project.

### Data Availability Statement

The data that support the findings of this study are available from the corresponding author upon reasonable request.

### Keywords

inverted perovskite solar cells, molecular design, ligands, non-radiative recombination, surface manipulation

Received: August 22, 2022  
Revised: September 27, 2022  
Published online:

- [1] R. Cheng, C. C. Chung, H. Zhang, F. Liu, W. T. Wang, Z. Zhou, S. Wang, A. B. Djurišić, S. P. Feng, *Adv. Energy Mater.* **2019**, 9, 1901980.
- [2] L. Rao, X. Meng, S. Xiao, Z. Xing, Q. Fu, H. Wang, C. Gong, T. Hu, X. Hu, R. Guo, Y. Chen, *Angew. Chem., Int. Ed.* **2021**, 60, 14693.
- [3] A. Al-Ashouri, E. Köhnen, B. Li, A. Magomedov, H. Hempel, P. Caprioglio, J. A. Márquez, A. B. M. Vilches, E. Kasparavicius, J. A. Smith, N. Phung, D. Menzel, M. Grischek, L. Kegelmann, D. Skroblin, C. Gollwitzer, T. Malinauskas, M. Jošt, G. Matič, B. Rech, R. Schlatmann, M. Topič, L. Korte, A. Abate, B. Stannowski, D. Neher, M. Stollerfoht, T. Unold, V. Getautis, S. Albrecht, *Science* **2020**, 370, 1300.
- [4] J. Y. Jeng, Y. F. Chiang, M. H. Lee, S. R. Peng, T. F. Guo, P. Chen, T. C. Wen, *Adv. Mater.* **2013**, 25, 3727.
- [5] Z. Li, B. Li, X. Wu, S. A. Sheppard, S. Zhang, D. Gao, N. J. Long, Z. Zhu, *Science* **2022**, 376, 416.
- [6] Q. Jiang, J. Tong, Y. Xian, R. A. Kerner, S. P. Dunfield, C. Xiao, R. A. Scheidt, D. Kuciauskas, X. Wang, M. P. Hautzinger, R. Tirawat, M. C. Beard, D. P. Fenning, J. J. Berry, B. W. Larson, Y. Yan, K. Zhu, *Nature* **2022**, 1.
- [7] M. Stollerfoht, C. M. Wolff, J. A. Márquez, S. Zhang, C. J. Hages, D. Rothhardt, S. Albrecht, P. L. Burn, P. Meredith, T. Unold, D. Neher, *Nat. Energy* **2018**, 3, 847.
- [8] M. Stollerfoht, P. Caprioglio, C. M. Wolff, J. A. Márquez, J. Nordmann, S. Zhang, D. Rothhardt, U. Hörmann, Y. Amir, A. Redinger, L. Kegelmann, F. Zu, S. Albrecht, N. Koch, T. Kirchartz, M. Saliba, T. Unold, D. Neher, *Energy Environ. Sci.* **2019**, 12, 2778.
- [9] J. Warby, F. Zu, S. Zeiske, E. Gutierrez-Partida, L. Frohloff, S. Kahmann, K. Frohna, E. Mosconi, E. Radicchi, F. Lang, S. Shah, F. Peña-Camargo, H. Hempel, T. Unold, N. Koch, A. Armin, F. De

- Angelis, S. D. Stranks, D. Neher, M. Stolterfoht, *Adv. Energy Mater.* **2022**, *12*, 2103567.
- [10] X. Zheng, B. Chen, J. Dai, Y. Fang, Y. Bai, Y. Lin, H. Wei, X. C. Zeng, J. Huang, *Nat. Energy* **2017**, *2*, 17102.
- [11] D. Luo, W. Yang, Z. Wang, A. Sadhanala, Q. Hu, R. Su, R. Shivanna, G. F. Trindade, J. F. Watts, Z. Xu, T. Liu, K. Chen, F. Ye, P. Wu, L. Zhao, J. Wu, Y. Tu, Y. Zhang, X. Yang, W. Zhang, R. H. Friend, Q. Gong, H. J. Snaith, R. Zhu, *Science* **2018**, *360*, 1442.
- [12] F. Li, X. Deng, F. Qi, Z. Li, D. Liu, D. Shen, M. Qin, S. Wu, F. Lin, S. H. Jang, J. Zhang, X. Lu, D. Lei, C. S. Lee, Z. Zhu, A. K. Y. Jen, *J. Am. Chem. Soc.* **2020**, *142*, 20134.
- [13] H. Chen, S. Teale, B. Chen, Y. Hou, L. Grater, T. Zhu, K. Bertens, S. M. Park, H. R. Atapattu, Y. Gao, M. Wei, A. K. Johnston, Q. Zhou, K. Xu, D. Yu, C. Han, T. Cui, E. H. Jung, C. Zhou, W. Zhou, A. H. Proppe, S. Hoogland, F. Laquai, T. Filleter, K. R. Graham, Z. Ning, E. H. Sargent, *Nat. Photonics* **2022**, *16*, 352.
- [14] X. Li, W. Zhang, X. Guo, C. Lu, J. Wei, J. Fang, *Science* **2022**, *375*, 434.
- [15] R. Azmi, E. Ugur, A. Seitkhan, F. Aljamaan, A. S. Subbiah, J. Liu, G. T. Harrison, M. I. Nugraha, M. K. Eswaran, M. Babics, Y. Chen, F. Xu, T. G. Allen, A. U. Rehman, C. Wang, T. D. Anthopoulos, U. Schwingenschlögl, M. D. Bastiani, E. Aydin, S. D. Wolf, *Science* **2022**, *376*, 73.
- [16] B. Chen, P. N. Rudd, S. Yang, Y. Yuan, J. Huang, *Chem. Soc. Rev.* **2019**, *48*, 3842.
- [17] S. Yang, J. Dai, Z. Yu, Y. Shao, Y. Zhou, X. Xiao, X. C. Zeng, J. Huang, *J. Am. Chem. Soc.* **2019**, *141*, 5781.
- [18] X. Zheng, Y. Hou, C. Bao, J. Yin, F. Yuan, Z. Huang, K. Song, J. Liu, J. Troughton, N. Gasparini, C. Zhou, Y. Lin, D. J. Xue, B. Chen, A. K. Johnston, N. Wei, M. N. Hedhili, M. Wei, A. Y. Alsalloum, P. Maity, B. Turedi, C. Yang, D. Baran, T. D. Anthopoulos, Y. Han, Z. H. Lu, O. F. Mohammed, F. Gao, E. H. Sargent, O. M. Bakr, *Nat. Energy* **2020**, *5*, 131.
- [19] J. Zhuang, P. Mao, Y. Luan, X. Yi, Z. Tu, Y. Zhang, Y. Yi, Y. Wei, N. Chen, T. Lin, F. Wang, C. Li, J. Wang, *ACS Energy Lett.* **2019**, *4*, 2913.
- [20] B. Li, Y. Xiang, K. D. G. I. Jayawardena, D. Luo, Z. Wang, X. Yang, J. F. Watts, S. Hinder, M. T. Sajjad, T. Webb, H. Luo, I. Marko, H. Li, S. A. J. Thomson, R. Zhu, G. Shao, S. J. Sweeney, S. R. P. Silva, W. Zhang, *Nano Energy* **2020**, *78*, 105249.
- [21] B. Li, W. Zhang, *Commun. Mater.* **2022**, *3*, 65.
- [22] S. Bouden, A. Dahi, F. Hauquier, H. Randriamahazaka, J. Ghilane, *Sci. Rep.* **2016**, *6*, 36708.
- [23] A. A. Sutanto, N. Drigo, V. I. E. Queloz, I. Garcia-Benito, A. R. Kirmani, L. J. Richter, P. A. Schouwink, K. T. Cho, S. Paek, M. K. Nazeeruddin, G. Grancini, *J. Mater. Chem. A* **2020**, *8*, 2343.
- [24] D. Meggiolaro, S. G. Motti, E. Mosconi, A. J. Barker, J. Ball, C. Andrea Riccardo Perini, F. Deschler, A. Petrozza, F. De Angelis, *Energy Environ. Sci.* **2018**, *11*, 702.
- [25] X. Yang, Y. Ni, Y. Zhang, Y. Wang, W. Yang, D. Luo, Y. Tu, Q. Gong, H. Yu, R. Zhu, *ACS Energy Lett.* **2021**, *6*, 2404.
- [26] Q. Jiang, Y. Zhao, X. Zhang, X. Yang, Y. Chen, Z. Chu, Q. Ye, X. Li, Z. Yin, J. You, *Nat. Photonics* **2019**, *13*, 460.
- [27] B. Philippe, M. Saliba, J. P. Correa-Baena, U. B. Cappel, S. H. Turren-Cruz, M. Grätzel, A. Hagfeldt, H. Rensmo, *Chem. Mater.* **2017**, *29*, 3589.
- [28] P. Caprioglio, F. Zu, C. M. Wolff, J. A. M. Prieto, M. Stolterfoht, P. Becker, N. Koch, T. Unold, B. Rech, S. Albrecht, D. Neher, *Sustain. Energy Fuels* **2019**, *3*, 550.
- [29] A. Al-Ashouri, A. Magomedov, M. Roß, M. Jošt, M. Talaikis, G. Khistiakova, T. Bertram, J. A. Márquez, E. Köhnen, E. Kasparavičius, S. Levenco, L. Gil-Escrig, C. J. Hages, R. Schlatmann, B. Rech, T. Malinauskas, T. Unold, C. A. Kaufmann, L. Korte, G. Niaura, V. Getautis, S. Albrecht, *Energy Environ. Sci.* **2019**, *12*, 3356.
- [30] S. N. Habisreutinger, N. K. Noel, H. J. Snaith, *ACS Energy Lett.* **2018**, *3*, 2472.
- [31] S. Wu, J. Zhang, Z. Li, D. Liu, M. Qin, S. H. Cheung, X. Lu, D. Lei, S. K. So, Z. Zhu, A. K. Y. Jen, *Joule* **2020**, *4*, 1248.
- [32] M. Degani, Q. An, M. M. Albaladejo-Siguan, Y. J. Hoffstetter, C. Cho, F. Paulus, G. Grancini, Y. Vaynzof, *Sci. Adv.* **2022**, *7*, eabj7930.
- [33] K. C. Hsiao, M. H. Jao, B. T. Li, T. H. Lin, S. H. C. Liao, M. C. Wu, W. F. Su, *ACS Appl. Energy Mater.* **2019**, *2*, 4821.
- [34] L. Meng, J. You, Y. Yang, *Nat. Commun.* **2018**, *9*, 5265.
- [35] M. V. Khenkin, E. A. Katz, A. Abate, G. Bardizza, J. J. Berry, C. Brabec, F. Brunetti, V. Bulović, Q. Burlingame, A. Di Carlo, R. Cheacharoen, Y. B. Cheng, A. Colmann, S. Cros, K. Domanski, M. Dusza, C. J. Fell, S. R. Forrest, Y. Galagan, D. Di Girolamo, M. Grätzel, A. Hagfeldt, E. von Hauff, H. Hoppe, J. Kettle, H. Köbler, M. S. Leite, S. (Frank) Liu, Y. L. Loo, J. M. Luther, et al., *Nat. Energy* **2020**, *5*, 35.
- [36] H. J. Snaith, A. Abate, J. M. Ball, G. E. Eperon, T. Leijtens, N. K. Noel, S. D. Stranks, J. T. Wang, K. Wojciechowski, W. Zhang, *J. Phys. Chem. Lett.* **2014**, *5*, 1511.
- [37] T. Zhang, S. H. Cheung, X. Meng, L. Zhu, Y. Bai, C. H. Y. Ho, S. Xiao, Q. Xue, S. K. So, S. Yang, *J. Phys. Chem. Lett.* **2017**, *8*, 5069.
- [38] P. Caprioglio, C. M. Wolff, O. J. Sandberg, A. Armin, B. Rech, S. Albrecht, D. Neher, M. Stolterfoht, *Adv. Energy Mater.* **2020**, *10*, 2000502.
- [39] T. Kirchartz, U. Rau, *Adv. Energy Mater.* **2018**, *8*, 1703385.